Selection criteria for the analysis of data-driven clusters in cerebral fMRI

C. Gómez-Laberge[1,2], A. Adler[2], I. Cameron[3], T. Nguyen[3], M.J. Hogan[*1]

[1] Neuroscience, Ottawa Health Research Institute, 451 Smyth Road, Ottawa, Ontario K1H 8M5, Canada

[2] Department of Systems and Computer Engineering, Carleton University, 1125 Colonel By Drive, Ottawa, Ontario K1S 5B6, Canada

[3] Department of Diagnostic Imaging, Ottawa Hosptial, 501 Smyth Road, Ottawa, Ontario K1H 8L6, Canada

[*] Corresponding author (email: mhogan@uottawa.ca)

Abstract

Functional MRI may be possible without *a priori* models of the cerebral hemodynamic response. First, such data-driven fMRI requires that all cerebral territories with distinct patterns be identified. Second, a systematic selection method is necessary to prevent the subjective interpretation the identified territories.

This study addresses the second point by proposing a novel method for the automated interpretation of identified territories in data-driven fMRI. Selection criteria are formulated using *i*) the temporal cross-correlation between each identified territory and the paradigm, and *ii*) the spatial contiguity of the corresponding voxel map. Ten event-design fMRI data sets are analysed with one prominent algorithm, fuzzy *c*-means clustering, before applying the selection criteria. For comparison, these data are also analysed with an established, model-based method: SPM.

Both methods produced similar results and identified potential activation in the expected territory of the sensorimotor cortex in all ten data sets. Moreover, the proposed method classified distinct territories in separate clusters. Selected clusters have a mean temporal correlation coefficient of 0.39 ± 0.07 ($n = 19$) with a mean 2.7 ± 1.4 second response delay. At most four separate contiguous territories were observed in 87% of these clusters. These results suggest that the proposed method may be effective for exploratory fMRI studies where the hemodynamic response is perturbed during cerebrovascular disease.

1 Introduction

Functional images of brain activation are obtained *indirectly* using the blood-oxygen-level dependent (BOLD) contrast during the course of an experimental paradigm. The challenge lies in the fact that the neurovascular relationship between neural activation and the hemodynamic variables describing cerebral blood flow (CBF), cerebral blood volume, and oxygen extraction fraction is not fully understood [1]. Thus, before a general theoretical model can be developed to describe the neurovascular relationship, the currently available methods aim to indentify cerebral territories of BOLD signal changes (often referred to as "activation maps") that are related to the experimental paradigm as an indicator of *potential* neural activity. Pathological cases evoke further problems, such as the severe perturbation of the cerebral hemodynamic regulation mechanism [2] and the occurrence of a natural inhibitor, which is known to de-couple the BOLD signal from neural activation [3].

Data-driven methods (or exploratory data analyses) are actively being studied as they enable the analysis and understanding of cerebral fMRI by identifying regions of potential neural activity without *a priori* models for the experimental paradigm, the hemodynamic response function (HRF), nor the underlying data structure under study. Several data-driven methods, broadly categorised as *clustering* algorithms, were compared based on quantitative figures-of-merit and found to be well-suited for fMRI analysis [4]–[7]. These techniques categorise voxels of fMRI data into several clusters, which are formed based on a measure of time sequence similarity, regardless of the experimental paradigm. Therefore, the task of inferring territories of potential neural activation from BOLD–paradigm related voxel maps must be systematically undertaken to prevent methodological errors and voxel map mis-interpretation [8]. That is, data-driven methods impose the requirement of a post-processing selection of clusters

that behave in relation to the experimental paradigm. Typically, this selection stage is done by humans with the condition that the interpretation is as objective and consistent as possible across data sets. Several groups have proposed in the literature selection criteria based on temporal measures within and between clusters [9] and on the degree of membership overlap that voxels have on fuzzy clusters [10], [11]. Criteria have also been proposed and studied based on distance measures between voxels and their centroids in the high-dimensional cluster space [12]. Indeed, these selection criteria introduce little *a priori* expectations on the underlying structure of the data related to the experimental paradigm.

In order to address the problem of objective post-processing cluster selection, this paper develops new and experimentally reasonable selection criteria based on *a priori* temporal knowledge of the experimental paradigm, as well as on spatial knowledge of the cerebrovascular network perfusing the brain. Once a data-driven method has analysed the image sequence, these criteria serve to quantitatively rank and select clusters whose member voxels are significantly responsive to an event-related paradigm and occupy contiguous regions of space in the brain. Experimental fMRI sessions involving visually cued motor tasks are first analysed using one prominent data-driven method: fuzzy c-means (FCM) cluster analysis [13], [9], as implemented in EvIdent (National Research Council, Winnipeg, Canada). The proposed criteria are then applied and the selected voxel maps are compared to an established, model-driven analysis method implemented in Statistical Parametric Mapping (SPM) (Wellcome Trust, London, United Kingdom).

2 Methods

2.1 fMRI acquisition and pre-processing

Ten experimental sessions acquired fMRI data from two healthy male volunteers of thirty-four and fifty-five years of age over a 6 month period using event-design paradigms. In each session, the subjects responded to a visual stimulus by executing simple hand motor-tasks briefly described in table 1. Before each imaging session, the subjects were instructed to perform the motor-tasks on "active" cues, and to relax on "rest" cues. The stimulus was a green horizontal bar displayed on a blue background, projected onto a screen in the MR room and viewed through a small mirror mounted in front of the subject's eyes. The bar was displayed in the lower part of the screen during "rest" states and would be quickly re-drawn in the upper part of the screen during "active" states. The paradigm state transitions were synchronised with the scanner's T_R cycles using an electronic trigger pulse emitted by the scanner at the start of each image acquisition. The recorded timing errors for these experiments were all under 10 ms.

The *open/close fist* and *finger tap* tasks were cued by this visual stimulus, but otherwise were uncontrolled. The *ball squeeze* task involves the subjects compressing a small plastic ball equipped with a pressure transducer. In this case, the stimulus also provides *visual feedback* when the subjects squeeze the ball so that they can control the amount of force applied. The visual feedback of the contraction force was provided graphically using LabVIEW v.8.2 (National Instruments, Austin, U.S.A.) by displaying a second (red) bar whose vertical position was proportional to the amount of force applied to the ball with added constraints to ensure the bar always remained on the screen.

All imaging was performed using a 1.5 Tesla Magnetom Symphony MR scanner (Siemens, Erlangen, Germany), wherein the subject lay supine with

their head secured. Localisation was performed using a T_1-weighted spin echo pulse sequence to align the slice selection gradient with pre-selected anatomical landmarks before functional imaging. Structural images were also acquired with this pulse sequence and a voxel size of $1.02 \times 1.02 \times 1.50$ mm^3. Whole brain echo planar fMRI was performed using a gradient echo pulse sequence ($T_R/T_E = 2000/30$ ms; 90°) and a voxel size of $1.56 \times 1.56 \times 5.00$ mm^3. Twenty-six transversal slices were acquired for each data set.

The event-design paradigm used in this study is illustrated in figure 1 and is described in [14]. The paradigm consisted of a random number of active/rest cycles between 12 and 15. Each cycle began with an active state of 2 T_R followed by a rest state between 8 and 10 T_R. A 10 T_R rest state took place before the first cycle. All paradigms were generated so as to acquire 160 images during each session.

Clinical research often requires inter-subject comparisons to make inferences on the population under study. Therefore, fMRI analysis methods should perform well on data first having undergone pre-processing for clinical analysis. The data in this study were pre-processed within SPM5 [15] as is typically done in our institute for inter-subject studies: i) the images were re-aligned to mitigate noise caused by head motion, ii) the images were normalised to the Montréal Neurological Institute (MNI) atlas to allow for inter-subject comparisons, and iii) the images were spatially smoothed using a Gaussian filter with kernel size 10 mm^3 to reduce the effect of high frequency noise on the analysis. The voxel size was unchanged during pre-processing, and the image matrix was changed from $128 \times 128 \times 26$ to $101 \times 122 \times 28$ voxels.

2.2 Fuzzy c-means clustering algorithm

After pre-processing, each session was analyzed using an implementation of the FCM algorithm in the software package EvIdent (National Research Council of Canada, Winnipeg) [16]. This particular implementation was chosen due to its adaptive cluster-merging feature, which reduces the sensitivity caused by the initial choice of the number of clusters [17]. The rationale behind the algorithm is to map voxel time sequences to vectors in a high-dimensional Euclidean space and cluster them based on mutual proximity. This section briefly reviews the algorithm's formulation.

Let K represent the number of clusters at any stage of the algorithm, let L be the number of voxels in an image, and let T be the number of images captured during the session. Furthermore, let $x_l[t]$ be the sequence of length T corresponding to the intensity of voxel l for $1 \leq l \leq L$. Similarly, let $v_k[t]$ be the sequence of same length corresponding to the centroid time sequence of cluster k for $1 \leq k \leq K$. Thus, any time sequence can be represented in a Euclidean space by the vector $\vec{x}_l = \langle x_l[1], \cdots, x_l[T] \rangle \in \mathbb{R}^T$.

Suitable proximity functions $d(x, v)$ are based on the distance and the angle between $\vec{x}$ and $\vec{v}$. We describe both available in EvIdent:

1. The distance measure is simply the Euclidean distance between vectors $d(x, v) = \|\vec{x} - \vec{v}\|$.

2. The Pearson product-moment correlation (PPMC) coefficient yields an angle measure between vectors $\vec{x}$ and $\vec{v}$ from their corresponding sequences

$$r(x, v) = \frac{\sum_{t=1}^{T}(x[t] - \bar{x})(v[t] - \bar{v})}{(T-1)s_x s_v}. \tag{1}$$

   The quantities $\bar{x}$ and s_x in equation (1) are the sample mean and sample standard deviation, respectively. The correlation-based measure called the

hyperbolic correlation distance [18] is a function mapping $r(x, v)$ onto the non-negative real numbers given by

$$d(x, v) = \sqrt{\frac{1 - r(x, v)}{1 + r(x, v)}}, \quad -1 < r(x, v) \leq 1. \tag{2}$$

We used the hyperbolic correlation distance, since previous studies demonstrated it to be more robust to noise and FCM sensitivity to initial parameters than the Euclidean distance [4], [18], [5]. Moreover, observe that equation (1) is directly proportional to the cosine of the angle, say θ, between the centred vectors $\vec{x} - \bar{x}$ and $\vec{v} - \bar{v}$; namely, $\cos\theta = (T - 1)r(x, v)$. Hence, unlike the Euclidean distance, correlation distances are invariant to the magnitude of the time sequence signal, and in turn, FCM produces fewer clusters and converges faster.

Given a proximity function $d(x, v)$ and two parameters (the fuzzy index $m > 1$ and the *initial* number of clusters K_0), FCM computes the following two calculations per iteration [9]:

1. For each vector, the cluster memberships are calculated using $d(x_l, v_k)$, such that we obtain the matrix $\mathbf{U}$ with elements

$$u_{kl} = \left[\sum_{n=1}^{K} \left(\frac{d(x_l, v_k)}{d(x_l, v_n)} \right)^{2/(m-1)} \right]^{-1} \tag{3}$$

   whose value $0 \leq u_{kl} \leq 1$ is the membership of voxel l to cluster k.

2. Given $\mathbf{U}$, the time sequence for each centroid $\vec{v}_k = \langle v_k[1], \cdots, v_k[T] \rangle$ is updated by computing the sequence elements

$$v_k[t] = \frac{\sum_{l=1}^{L} (u_{lk})^m x_l[t]}{\sum_{l=1}^{L} (u_{lk})^m}, \quad \text{for } t = 1, \ldots, T. \tag{4}$$

Equations (3) and (4) iteratively minimise the objective function

$$J(\mathbf{U}, \mathbf{V}, \mathbf{X}) = \sum_{k=1}^{K} \sum_{l=1}^{L} u_{kl}^{m} d^2(x_l, v_k), \tag{5}$$

where $\mathbf{V} = [v_1, \cdots, v_K]$ and $\mathbf{X} = [x_1, \cdots, x_L]$. An adaptive cluster-merging feature described in [17] is used after each iteration, which merges two mutually proximal clusters based on the similarity of their membership values, calculated in the corresponding rows of $\mathbf{U}$. Once the algorithm converges on K final clusters, each voxel is categorically assigned to the cluster C_k providing the maximum membership. That is, the mutually exclusive clusters are the sets of voxels given by

$$C_k = \left\{ x_l : \max([\mathbf{U}]_{\text{col } l}) = u_{kl} \right\}, \quad \text{for } k = 1, \ldots, K. \tag{6}$$

No subregions of interest were selected in any of the analyses; the algorithm was initialised with 35 clusters and was observed to converge within 20 iterations. A fuzzy index of $m = 1.1$ was used instead of the recommended value of 2 [11]. Inspection of the FCM results from EvIdent showed a progressive reduction in the number of clusters as m increased from 1.1 to 2 as distinct clusters were merged. The compromise of obtaining more distinct clusters is the introduction of spurious voxels into each cluster, potentially increasing the false-positive error rate. The rationale we take prioritises the indentification of distinct clusters from FCM, which are significantly related to the paradigm, however having subtle differences in temporal and spatial characteristics. The post-processing stage, described next, imposes criteria on the FCM output to select contiguous regions of cerebral territories identified in clusters that are significantly correlated to the paradigm.

2.3 Selection criteria for the interpretation of voxel maps

No *a priori* information is used to cluster similar voxels. Instead, patterns in the data are identified by grouping similar time sequences, regardless of their cause. Such approaches typically show clusters which identify various physiological and instrument-based effects taking place during image acquisition; some of which may be responsive to the paradigm stimulus and to brain function.

In this section, we propose criteria for the automated interpretation and selection of the clusters obtained from a data-driven analysis whose voxels are significantly responsive to the paradigm stimulus and occupy a contiguous regions in the brain. Briefly, clusters are interpreted in a two-stage process described in detail in sections 2.3.1 and 2.3.2. First, all K centroids are compared to the paradigm design by calculating their time sequence cross-correlation function. The centroids exhibiting a significant correlation, with a possible phase delay, are selected as representing voxels that are responding to the paradigm. Second, the member voxels of the selected clusters are scrutinised based on a novel spatial contiguity criterion. The voxels selected by these criteria are identified as regions of potential neural activation during the stimulus.

2.3.1 Temporal criterion: cluster–paradigm cross-correlation

By modelling the state transitions of the paradigm as a time sequence, a comparison is possible between the temporal behaviour of a cluster centroid with the paradigm by calculating the cross-correlation function. Since phase shifts due to response delays or habituation are expected, the cross-correlation is meaningful as it quantifies the correlation between two signals as a function phase shift. Although this criterion is useful in quantifying a temporal relationship for simple paradigms, it is difficult to extend to multiple-state designs, since there is no rationale for assigning arbitrary values to the various states in the paradigm

sequence. Hence, this criterion applies to simple event-related paradigms consisting of only two states.

The centroid time sequences $v_k[t]$ for $k = 1, \ldots, K$ are compared to the paradigm time sequence $p[t]$, also of length T, which models the paradigm described in section 2.1. During "rest" and "active" states, the paradigm time sequence takes values zero and one, respectively. The cross-correlation between two sequences $v[t]$ and $p[t]$ is the sequence $(v \star p)[d]$ of length $2T - 1$, with elements defined as

$$(v \star p)[d] = \sum_{t=1}^{T} v[t + d - T]p[t], \quad d = 1, \ldots, 2T - 1. \tag{7}$$

Similar to the property in equation (1), it can be shown that

$$(v \star p)[d] = (T - 1)s_v s_p r(v^{(d-T)}, p) \quad \text{for } 1 \leq d < 2T, \tag{8}$$

where $v^{(d)}[t] = v[(t + d) \mod T]$ is a circular shift of d elements. Using equation (7), all centroids are ranked by largest maximum cross-correlation for $T \leq d \leq T + \tau_{\text{rest}}$, where τ_{rest} is the minimum rest period in the paradigm. This constraint is used for ensuring that each response is cross-correlated of with its corresponding stimulus. Interestingly, clusters with negatively correlated centroids have been observed in previous BOLD fMRI studies. The possiblity of long delays causing negative correlations was examined and ruled out, leaving several physiological hypotheses such as an unexpected increase in vascular concentrations of deoxyhemoglobin or an inverse BOLD constrast [4]. Hence, we equally consider clusters with negatively correlated centroids as responsive to the paradigm. Finally, the criterion requires that clusters containing regions that are potentially activated by the paradigm have a cluster–paradigm correlation coefficient $|r(v[t + d], p[t])| \geq 0.30$. A coefficient threshold of 0.30 is

suggested for "medium or strong" correlations according to experimental statistical guidelines [19].

2.3.2 Spatial criterion: voxel map contiguity

The cerebral vasculature perfuses contiguous volumes of tissue *via* common networks of arterioles. The regulation of CBF is locally undertaken by the constriction and dilation of the pre-capillary arterioles; therefore, neural activity is thought to occur in contiguous regions of tissue [20]. Consequently, the BOLD signal is also expected to emerge as a contiguous spatial distribution of voxels in fMRI. Based on the above, this spatial criterion seeks clusters containing sets of contiguous voxels.

The data acquired within the scanner is a discrete sampling of the volume field of view over time. Each sample can be considered as the point represented by its enclosing voxel. A more convenient notation for spatial analysis is to write $x_l[t]$, the time sequence of voxel l, as $x[\vec{n}_l, t] = x[n_x, n_y, n_z, t]$. Now any voxel is denoted by its spatial coordinates $\vec{n} = \langle n_x, n_y, n_z \rangle$ on the lattice $\Lambda = \left\{ \mathbf{V}\vec{n} \,\middle|\, \vec{n} \in \mathbb{Z}^3 \right\}$, where $\mathbf{V}$ is the diagonal matrix voxel dimensions $\mathbf{V} = \mathbf{I}_3 \langle X\,\text{mm}, Y\,\text{mm}, Z\,\text{mm} \rangle^\top$.

The clusters selected by the temporal criterion have centroids that are significantly correlated to the paradigm design. The centroids are calculated as in equation (4) and, therefore, are membership-weighted linear combinations of the member voxel time sequences. Hence, the clusters reveal how the member voxels are distributed in space as a function of correlation with the centroid. Using equation (1) for each cluster C_k, we define a correlation function that produces the PPMC coefficients for each member voxel of C_k

$$R_k[\vec{n}] = \begin{cases} r(x[\vec{n}_l], v_k) & \text{for } x_l \in C_k, \\ 0 & \text{otherwise.} \end{cases} \tag{9}$$

Given $R_k[\vec{n}]$ for $k = 1, \ldots, K$, contiguous clusters can be potentially distinguished from sporadic ones. This requires that *contiguity* be quantitatively defined; thus, we propose the following notions leading to a definition of contiguity.

Two voxels who share the same face are said to be *adjacent*, and one unbroken sequence of adjacent voxels is defined as a *group*. All L voxels of any cluster can be counted group-wise by the series

$$L = 1g_1 + 2g_2 + \cdots + Mg_M, \tag{10}$$

where g_l is the number of groups of l voxels, and the largest group has M voxels. We consider a group to be *contiguous* if it contains a number of voxels equal or greater than some constant m. Thus, by setting $g_l = 0$ for $l < m$, we obtain the fraction of L voxels belonging to contiguous groups

$$0 \leq \frac{1}{L} \sum_{l=m}^{M} l g_l \leq 1. \tag{11}$$

Finally, to penalise clusters with a large number, say G, of groups, the series is normalised by the product GL instead of simply L. Therefore, the contiguity of a cluster as defined above is given by the series

$$c = \frac{1}{GL} \sum_{l=m}^{M} l g_l. \tag{12}$$

Indeed, it is not unusual to expect multiple distinct cerebral territories interacting during the execution of a task. However, we expect that this number of distinct territories be lower, and thus receiving smaller penalty, than a sporadic number of small regions grouped together by chance during the data-driven analysis. Figure 2 illustrates the contiguity values obtained from equation (12)

with $m = 3$ for a set of two-dimensional fictional clusters. For the five clusters shown, the total number of voxels in each is the same: $L = 14$. This measure of contiguity is bounded between [0,1] and increases with fewer, larger groups. For example, the third cluster has two contiguous groups: one with three voxels, the other with nine voxels. Thus, the contiguity accoring to equation (12) is $c = (1 \times 3 + 1 \times 9)/(2 \times 14) = 0.43$. The measure is independent of voxel size, as long as m is scaled by the volume ratio between sizes. For three-dimensional fMRI data, we defined the smallest contiguous group using $m = 6$.

Before applying equation (12) to the set of voxels in each cluster, it is important to consider the nature of cluster membership in terms of correlation. The centroid computed in equation (4) is a weighted average of the member voxel time sequences, where very similar voxel sequences are assigned large weight coefficients calculated using equation (3). When comparing the centroid with all member voxels, only few will have large coefficients, and progressively more will have lower coefficients. However, a lower limit must exist where $\min_{x_l \in C_k} R_k[\vec{n}] > 0$, since no *member* voxel can be uncorrelated to the centroid, by definition. Therefore, for each cluster, we can obtain a bounded distribution of the contiguity over the domain of correlation coefficients: $c = c(r)$, for $0 \leq r \leq 1$. We use the median value of each cluster's contiguity distribution as a lower threshold limit r_{th} for the selection of member voxels. Finally, in each cluster, the spatial criterion selects the subset of member voxels for which $R_k[\vec{n}] \geq r_{\text{th}}$ and displays the resulting voxel map.

3 Results

The proposed criteria were applied to the ten fMRI sessions described above in table 1. The expected territory of paradigm-correlated BOLD signal is in the sensorimotor cortex (*i.e.*, the pre-central gyrus on the frontal lobe contralateral

to the responding hand). A secondary expected territory is the visual cortex (*i.e.*, the posterior occiptial lobe). These expected territories were selected by neurologists, and all sessions were also independently analysed with a first-level SPM t-test (two-tailed) with familywise error probability of $p < 0.05$. The following sections report inter- and intra-session comparisons between methods including observations on the proposed method's performance.

3.1 Inter-session comparison

The proposed method and SPM both identified significant voxels in the motor cortex for all sessions. The visual cortex, however, was identified in roughly half of the sessions by either method (proposed method 5/10, SPM 6/10). The results from the proposed method for all sessions are given in table 2. The heading in bold type shows how many clusters were selected from the total number of clusters formed by FCM algorithm. In each row, the details of the selected clusters are given: the cluster number, the number of member voxels (L), the cluster–paradigm correlation (r), the response delay (d) of the cluster centroid in T_R, and the contiguity evaluated using member voxels above the cluster's PPMC threshold $c(r_{\text{th}})$. The last column lists gross cerebral territories identified by the cluster. Clusters prefixed with the symbol '▶' identified voxels in the motor cortex.

Some observations can be made looking at these results. The proposed method can identify multiple clusters, representing distinguishable voxel groups that are responsive to the stimulus. Using the cluster–paradigm correlation threshold $|r| \geq 0.30$, the correlated clusters indentified in the cerebrum, across all sessions, have a mean correlation $\bar{r} = 0.39 \pm 0.07$ ($n = 19$). These also exhibited the expected 2% increase of the BOLD signal upon stimulus. In addition, the proposed method also identified clusters with strong negative correlations

$\bar{r} = -0.53 \pm 0.12$ ($n = 12$). These occurr almost exclusively in the eye orbits with the exception of motor cortex voxels from cluster 23 in session 7, where a weaker inverted signal was identified with $r = -0.34$. We presume that eye orbit voxels emerged from eye movements, while the subject followed the moving target on the stimulation screen. Although an inverse BOLD response has been observed in the literature [4], we have not attempted to control our experiments for such an effect. Further comparison of the voxel time sequences of each cluster reveals characteristic differences in the BOLD signal amplitude and response delay. For example, the peak-to-peak amplitude of responsive cortical voxels ranged between 0.5% to 2% of signal strength, while the ampliude of the orbit voxels ranged between 10% to 20%. The response delays shown in table 2 have a response delay of $\bar{d} = 2.74 \pm 1.37$ seconds ($n = 19$) for all cerebral voxels. This is plausible considering the latencies of the hemodynamic response reported between 2-4 seconds (including the intial signal dip) [1]. The voxels corresponding to the eye orbits have no measurable delay, which also supports our assumption of artefact from eye movements during stimulus onset. Twenty-seven selected clusters contain voxels in one gross territory and have contiguity values larger than 0.25 (*i.e.*, contiguous voxel groups per cluster ≤ 4). The remaining four clusters, from sessions 9 and 10, contain several territories and, hence, fall well below this value.

3.2 Intra-session comparison

To illustrate further details, figure 3 compares the voxel maps obtained from an SPM t-test and the proposed method using the data from session 9. Although the same cerebral territories were identified, some rather prominent differences were observed. To elucidate these differences, the first row of figure 3 shows the SPM map from a less conservative SPM t-test with a type I error rate

of $p < 0.001$ without familywise correction. Applying the conservative t-test that was used for the inter-session comparison would retain only the darkest regions of the SPM voxel map shown in this figure. The SPM map reveals significant voxels in the expected motor cortex (left posterior frontal lobe), the occipital lobe, and the cerebellum. Regions shown in a lighter shade correspond mostly to the superior sagittal sinus; other smaller sporadic regions also emerge throughout the brain. The remaining rows show the clusters from the proposed method. Figure 4 shows the corresponding cluster–paradigm correlation and contiguity plots for these clusters. Clusters 20, 21, and 9 have identified voxels in the cerebellum, the motor cortex, and the occipital lobe, respectively. These clusters seem to overlap well with the SPM map; however, there is a prominent mismatch in the superior part of the motor cortex. For comparison, territories identified by each cluster have been circled on the SPM map in the cluster map's corresponding colour. The lateral part of the motor cortex identified by both methods (shown in cluster 21) is also marked with the symbol '<' on the SPM map. Cluster 13 (shown in the last row) contains the superior motor cortex; however, it was rejected by the proposed criteria having cluster–paradigm correlation $r = 0.26 < 0.30$. Cluster 13 is less contiguous ($c(0.75) = 0.07$) than the selected clusters, containing areas along the superior sagittal sinus, the frontal and parietal cortices ipsilateral to the responding hand, and the inferior occipital lobe. On the other hand, although the centroid has low correlation with the paradigm, it has rather well defined peaks and troughs and shows some degree of relationship to the paradigm. Indeed, parameter selection will not fit all cases, and by relaxing the suggested threshold $|r| \geq 0.30$, one admits this and other sporadic clusters.

4 Discussion

This study proposed a method for the systematic selection of voxel maps identifying potentially activated cerebral territories obtained from an FCM analysis of fMRI data. Selection criteria were proposed for the automated interpretation and selection of the clusters obtained from a data-driven analysis, whose voxels are significantly responsive to the paradigm stimulus and occupy contiguous regions in the brain.

Interestingly, the temporal cross-correlation between centroids and the paradigm was previously recommended by Goutte *et al.* [4] in a pre-processing stage. The correlation values and corresponding phase delays served as an alternative to raw BOLD data in k-means clustering to reduce the algorithm's sensitivity to the fixed number of clusters and to mitigate scanner noise. Although this may be highly relevant for k-means clustering, this method was not used here. Instead, noise was reduced using image re-alignment and Gaussian low-pass filtering; algorithm sensitivity was handled by the adaptive cluster-merging feature in EvIdent [17]. A similar approach to the proposed temporal criterion, suggested by Chuang *et al.* [5], automatically selects the voxel maps whose centroids have a high correlation coefficient with the paradigm. However, the techniques for determining a suitable threshold level or for handling phase delays were not presented. One known challenge in temporal analysis of fMRI is modelling complex paradigms. The proposed temporal criterion is limited to simple paradigms, where a sequence of "rest" and "active" states can be modelled by values 0 and 1. However, there is no rationale for assigning arbitrary values to several states mixed together in a complex paradigm sequence. Randomly occurring event-related designs present some intuitive advantages over the blocked designs, which prompted our choice of paradigm. First, randomly occurring events form an aperiodic design and diminish the response anticipation effects

observed in periodic designs. Second, brief events diminish habituation effects observed during sustained activity. Finally, an aperiodic response is easier to distinguish from artefact signals caused by periodic physiological processes; *e.g.*, breathing and cardiac cycle effects.

To our knowledge, no other similar spatial criterion appears in the literature. The motivation for developing a spatial criterion is that data-driven analyses aim to identify all patterns in the dataset, without *a priori* knowledge of the experiment. In the case of the FCM algorithm, clusters are formed based on temporal correlation between the voxel time sequences and the centroids. Using fMRI data, we often observe clusters containing collections of sporadic voxels, each with time sequences that are weakly correlated to both the centroid and the paradigm. These are likely due to experimental noise, whence a realisation of voxel time sequences having small correlation coefficients appear in voxel maps like "salt-and-pepper". Since these cluster members are non-responsive to the paradigm and cannot be associated with any cerebral terrirory, they are of little interest to the analyst. Hence, by examining the spatial distribution of a cluster, one can remove the addition of weakly correlated sporadic voxels. Furthermore, such a contiguity measure imposes no geometrical restraint beyond the requirement that voxels be *connected* together. Hence, contiguous groups that have enlongated, spherical, or flat shape are treated alike. This would be difficult to achieve for example with a low-pass filtering approach, since multiple kernels would be necessary to account for an arbitrary shape.

Before the interpretation of a data-driven analysis, care is required to ensure that the algorithm converges properly. A methodological study by Möller *et al.* demonstrates that an insufficient convergence of the algorithm during the analysis stage produces unrepresentative clusters, which lead to the misinterpretation of the experiment [22]. In this study, we ensured the FCM algorithm

converged for each session by manually verifying several items: i) the number of iterations does not meet the allowed maximum, ii) the number of clusters does not reach the allowed minimum or maximum on any iteration, and iii) the voxel time sequences maintain similarity within clusters upon termination of the analysis. For efficiency, larger studies can integrate an automation of the protocol described in [22].

The method was applied to ten experimental sessions that were analysed by the FCM algorithm in EvIdent. The selected voxel maps were compared to a multiple comparison t-test analysis in SPM. Both methods identified potential neural activation in the expected motor cortex territory in all sessions and the expected visual cortex territory in roughly half of the sessions. Some differences between the voxel maps from each method were observed, particularly when a cluster is rejected having a sub-threshold correlation with the paradigm. Indeed, voxels failing to achieve either a p-value or a correlation r threshold, may still contain useful information and *vice versa*. The proposed method demonstrated the potential to distinguish several responsive areas using multiple clusters. Thus, individual information about one potential region of activation are not mixed with identified voxels in other regions. This observation demonstrates the potential that data-driven methods can expose highly relevant temporal and spatial characteristics of these regions. Such information may be useful in studying HRF behaviour perturbed by cerebrovascular disease in distinct regions of the brain.

In addition to the FCM algorithm, other fMRI analysis methods have been reported in the literature that may benefit form the proposed selection criteria. They can be broadly classified as *linear* methods based on a decomposition of the data into linear components, and *non-linear* methods based on the iterative clustering of data points with similar characteristics. Two independent compar-

ative studies on the performance of several methods were carried out in 2004 by Dimitriadou *et al.* and by Mayer-Baese *et al.* [7] [6]. Performance figures-of-merit were based on contingency tables (ROC analysis) and voxel time sequence accuracy in the activated region using artificial activation signals embedded in either simulated or real fMRI data. Both studies found that the non-linear algorithm *neural gas* performed best in identifying the active voxels. They disagreed, however, in their evaluation of the FCM algorithm. In terms of *neural gas*, one claimed it had comparable performance, while the other claimed its performance was significantly lower. Both studies concluded that the efficacy of non-linear methods is superior to that of linear methods.

The development of data-driven fMRI analysis methods has gained impetus due to the exploratory nature of research involving cerebral fMRI. The recourse of eschewing *a priori* models is attractive, since a quantitative relationship between cerebrovascular, metabolic, and neural parameters remains a highly pursued topic.

5 Acknowledgements

The authors would like to thank W. M. Czura for his work on the hardware and software implementations for the stimulation apparatus. This research was supported by BRAIN (Behavioural Research and Imaging Network) in partnership with the Ontario Research Fund, and by the Heart and Stroke Foundation Centre for Stroke Recovery.

References

[1] R. B. Buxton, K. Uludağ, D. J. Dubowitz, and T. T. Liu, "Modeling the hemodynamic response to brain activation," *NeuroImage*, vol. 23, pp. S220-

S233, 2004.

[2] H. Girouard and C. Iadecola, "Neurovascular coupling in the normal brain and in hypertension, stroke, and Alzheimer disease," *J. Appl. Physiol.*, vol. 100, pp. 328-335, 2006.

[3] M. Burke and Ch. Bührle, "BOLD response during uncoupling of neuronal activity and CBF," *NeuroImage*, vol. 32, pp. 1-8, 2006.

[4] C. Goutte, P. Toft, E. Rostrup, F. Å. Nielsen, and L. K. Hansen, "On clustering fo fMRI time series," *NeuroImage*, vol. 9, pp. 298-310, 1999.

[5] K.-H. Chuang, M.-J. Chiu, C.-C. Lin, and J.-H. Chen, "Model-free functional MRI analysis using Kohonen clustering neural network and fuzzy c-means," *IEEE Trans. Med. Imag.*, vol. 18, pp. 1117-1128, 1999.

[6] A. Meyer-Baese, A. Wismueller, and O. Lange, "Comparison of two exploratory data analysis methods for fMRI: unsupervised clustering versus independent component analysis," *IEEE Trans. Info. Tech. Biomed.*, vol. 8, pp. 387-398, 2004.

[7] E. Dimitriadou, M. Barth, C. Windischberger, K. Hornik, and E. Moser, "A quantitative comparison of functional MRI cluster analysis," *Artif. Intell. Med.*, vol. 31, pp. 57-71, 2004.

[8] M. M. Machulda, H. A. Ward, R. Cha, P. O'Brien, and C. R. Jack, "Functional inferences vary with the methodology," *NeuroImage*, vol. 14, pp. 1122-1127, 2001.

[9] J. C. Bezdek, *Pattern Recognition with Fuzzy Objective Function Algorithms*, New York, USA: Plenum Press, 1981, pp. 256.

[10] M. J. Fadili, S. Ruan, D. Bloyet, and B. Mazoyer, "A multistep unsupervised fuzzy clustering analysis of fMRI time series," *Hum. Brain Mapp.*, vol. 10, pp. 160-178, 2000.

[11] M. J. Fadili, S. Ruan, D. Bloyet, and B. Mazoyer, "On the number of clusters and the fuzziness index for unsupervised FCA application to BOLD fMRI time series," *Med. Imag. Anal.*, vol. 5, pp. 55-67, 2001.

[12] X. Wang, Y. Wang, L. Wang, "Improving fuzzy c-means clustering based on feature-weight learning," *Pattern Recog. Letters*, vol. 25, pp. 1123-1132, 2004.

[13] J. C. Dunn, "Some recent investigations of a new fuzzy partition algorithm and its application to pattern classification problems," *J. Cybernetics*, vol. 4, pp. 1-15, 1974.

[14] S. A. Huettel, A. W. Song, and G. McCarthy, *Functional Magnetic Resonance Imaging*, Sunderland, USA: Sinauer Associates, 2004, pp. 492.

[15] J. Ashburner, *Computational Neuroanatomy*, Ph.D. thesis, University College London, 2000.

[16] M. Jarmasz and R. L. Somorjai, "Exploring regions of interest with clustering analysis (EROICA) using a spectral peak statistic for selecting and testing the significance of fMRI activation time series," *Artif. Intell. Med.*, vol. 25, pp. 45-67, 2002.

[17] M. Jarmasz and R. L. Somorjai, "Time to join! Cluster-merging in unsupervised fuzzy clustering of functional MRI data," *Proc. ISMRM 6th Annu. Meeting*, Sydney, Australia, 1998, p.2068.

[18] X. Golay, S. Kollias, G. Stoll, D. Meier, A. Valavanis, and P. Boesiger, "A new correlation-based fuzzy logic clustering algorithm for fMRI," *Magn. Reson. Med.*, vol. 40, pp. 249-260, 1998.

[19] J. Cohen, *Statistical power analysis for the behavioral sciences* (2nd ed.), Hillsdale, USA: Laurence Erlbaum Associates, 1988, pp. 567.

[20] W. Kuschinsky, "Regulation of Cerebral Blood Flow," *Functional MRI* (Eds. Moonen, C.T.W., Bandettini, P.A.), Germany: Springer, 2000, pp. 15-24.

[21] D. C. Howell, *Statistical methods for psychology* (3rd ed.), Belmont, USA: Duxbury Press, 1992, pp. 693.

[22] U. Möller, M. Ligges, P. Georgiewa, C. Grünling, W. A. Kaiser, H. Witte, and B. Blanz, "How to avoid spurious cluster validation? A methodological investigation on simulated and fMRI data," *NeuroImage*, vol. 17, pp. 431-446, 2002.

Table 1: Summary of paradigm and motor task

Session	*Motor task*	*Hand*	*Visual feedback*
1	open/close fist	right	no
2	index finger tap	right	no
3	ball squeeze 15% max. force	left	yes
4	ball squeeze 15% max. force	right	yes
5	ball squeeze 50% max. force	right	yes
6	ball squeeze 100% max. force	right	yes
7	ball squeeze 15% max. force	left	yes
8	ball squeeze 15% max. force	right	yes
9	ball squeeze 50% max. force	right	yes
10	ball squeeze 100% max. force	right	yes

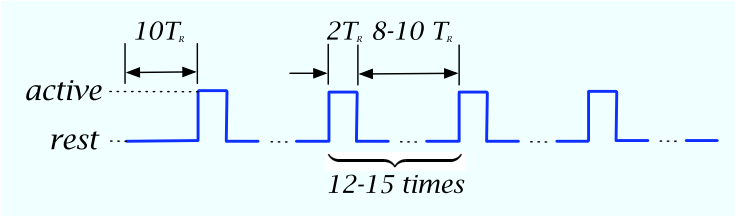

Figure 1: Schema of the event-design paradigm used in this study ($T_R = 2.00$ s).

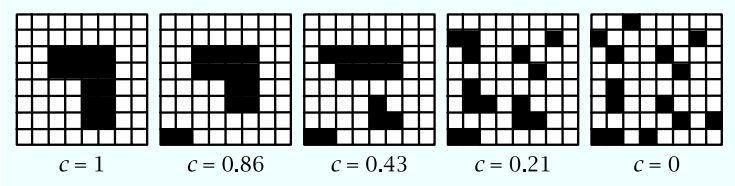

Figure 2: Contiguity c for a collection of 2D clusters. In each case, the total number of member voxels is $L = 14$, and the smallest group size is set to $m = 3$.

Table 2: List of selected clusters with their size, paradigm correlation, response delay, and contiguity. The territories identified in each cluster (predominant listed in bold type) are abbreviated using l = left, r = right, bi = bilateral, and SMC = sensorimotor cortex, FC = frontal cortex, PC = parietal cortex, OC = occipital cortex, CB = cerebellum, CG = cingulate gyrus, EYE = eye orbit, OTHER = other. The cluster identifying the expected SMC is preceded by ▶.

Session 1: criteria selected 6 of 23 clusters					
▶Cluster 2	$L = 1293$	$r = 0.45$	$d = 2$	$c(0.63) = 0.33$	**lSMC** lFC rSMC
Cluster 6	$L = 225$	$r = 0.44$	$d = 1$	$c(0.78) = 1$	**rOC**
Cluster 7	$L = 1195$	$r = 0.34$	$d = 2$	$c(0.77) = 0.50$	**biCB** biOC
Cluster 18	$L = 322$	$r = 0.31$	$d = 2$	$c(0.75) = 0.50$	**biPC**
Cluster 14	$L = 120$	$r = 0.30$	$d = 1$	$c(0.83) = 1$	**lOC**
Session 2: criteria selected 1 of 7 clusters					
▶Cluster 1	$L = 1078$	$r = 0.40$	$d = 2$	$c(0.67) = 0.33$	**lSMC**
Session 3: criteria selected 1 of 30 clusters					
▶Cluster 10	$L = 206$	$r = 0.54$	$d = 1$	$c(0.77) = 1$	**rSMC**
Session 4: criteria selected 1 of 12 clusters					
▶Cluster 10	$L = 217$	$r = 0.35$	$d = 2$	$c(0.64) = 1$	**lSMC**
Session 5: criteria selected 1 of 14 clusters					
▶Cluster 9	$L = 1253$	$r = 0.34$	$d = 1$	$c(0.72) = 0.25$	**lSMC** rSMC biFC
Session 6: criteria selected 2 of 11 clusters					
Cluster 9	$L = 368$	$r = 0.40$	$d = 2$	$c(0.78) = 1$	**OTHER**
▶Cluster 7	$L = 162$	$r = 0.49$	$d = 1$	$c(0.82) = 0.31$	**lSMC** rSMC biFC
Session 7: criteria selected 5 of 27 clusters					
Cluster 1	$L = 860$	$r = -0.59$	$d = 0$	$c(0.64) = 0.25$	**EYE**
Cluster 24	$L = 292$	$r = -0.51$	$d = 0$	$c(0.77) = 0.33$	**EYE**
Cluster 27	$L = 56$	$r = 0.41$	$d = 0$	$c(0.70) = 0.97$	**EYE**
Cluster 20	$L = 457$	$r = 0.45$	$d = 1$	$c(0.68) = 1$	**biCG**
▶Cluster 23	$L = 215$	$r = -0.34$	$d = 2$	$c(0.72) = 1$	**rSMC** (slightly anterior)
Session 8: criteria selected 4 of 12 clusters					
Cluster 1	$L = 479$	$r = -0.70$	$d = 0$	$c(0.64) = 0.25$	**EYE**
Cluster 5	$L = 329$	$r = -0.48$	$d = 0$	$c(0.72) = 0.247$	**EYE**
Cluster 2	$L = 471$	$r = -0.55$	$d = 0$	$c(0.59) = 0.50$	**EYE**
▶Cluster 11	$L = 4355$	$r = 0.33$	$d = 3$	$c(0.51) = 0.20$	**biOC** lSMC
Session 9: criteria selected 5 of 23 clusters					
Cluster 3	$L = 958$	$r = -0.62$	$d = 0$	$c(0.64) = 0.25$	**EYE**
Cluster 20	$L = 296$	$r = 0.43$	$d = 1$	$c(0.75) = 0.25$	**rCB** lCB
Cluster 14	$L = 284$	$r = -0.40$	$d = 0$	$c(0.83) = 0.33$	**EYE**
▶Cluster 21	$L = 283$	$r = 0.38$	$d = 2$	$c(0.71) = 0.19$	**lSMC**
Cluster 9	$L = 2050$	$r = 0.31$	$d = 2$	$c(0.71) = 0.14$	**rOC** CER
Session 10: criteria selected 6 of 13 clusters					
Cluster 1	$L = 422$	$r = -0.65$	$d = 0$	$c(0.62) = 0.32$	ORB
Cluster 8	$L = 287$	$r = -0.68$	$d = 0$	$c(0.58) = 0.50$	CER
▶Cluster 6	$L = 8959$	$r = 0.49$	$d = 1$	$c(0.68) = 0.05$	**OTHER** (incl. lSMC biOC)
Cluster 2	$L = 333$	$r = -0.44$	$d = 0$	$c(0.62) = 0.50$	**EYE**
Cluster 3	$L = 377$	$r = -0.36$	$d = 0$	$c(0.73) = 0.25$	**EYE**
Cluster 5	$L = 2961$	$r = 0.33$	$d = 0$	$c(0.62) = 0.05$	**OTHER** biFC

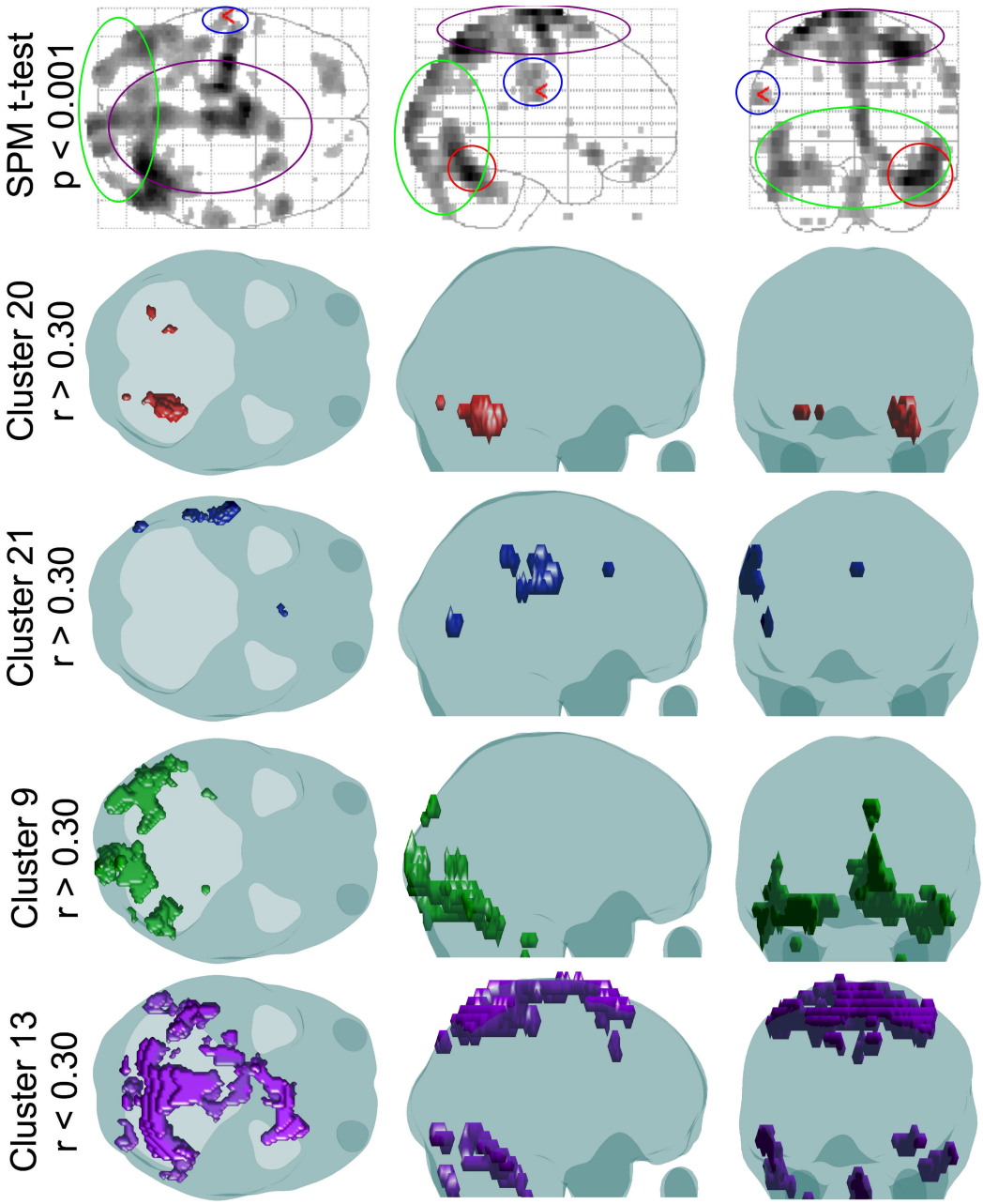

Figure 3: Comparison between the SPM t-test $p < 0.001$ (top row) and the proposed method (four clusters in remaining three rows) for session 9 data. Each map is displayed in transcranial (superior view), sagittal (right view), and coronal (posterior view) projections. Territories identified by each cluster have been circled on the SPM map in the corresponding colour.

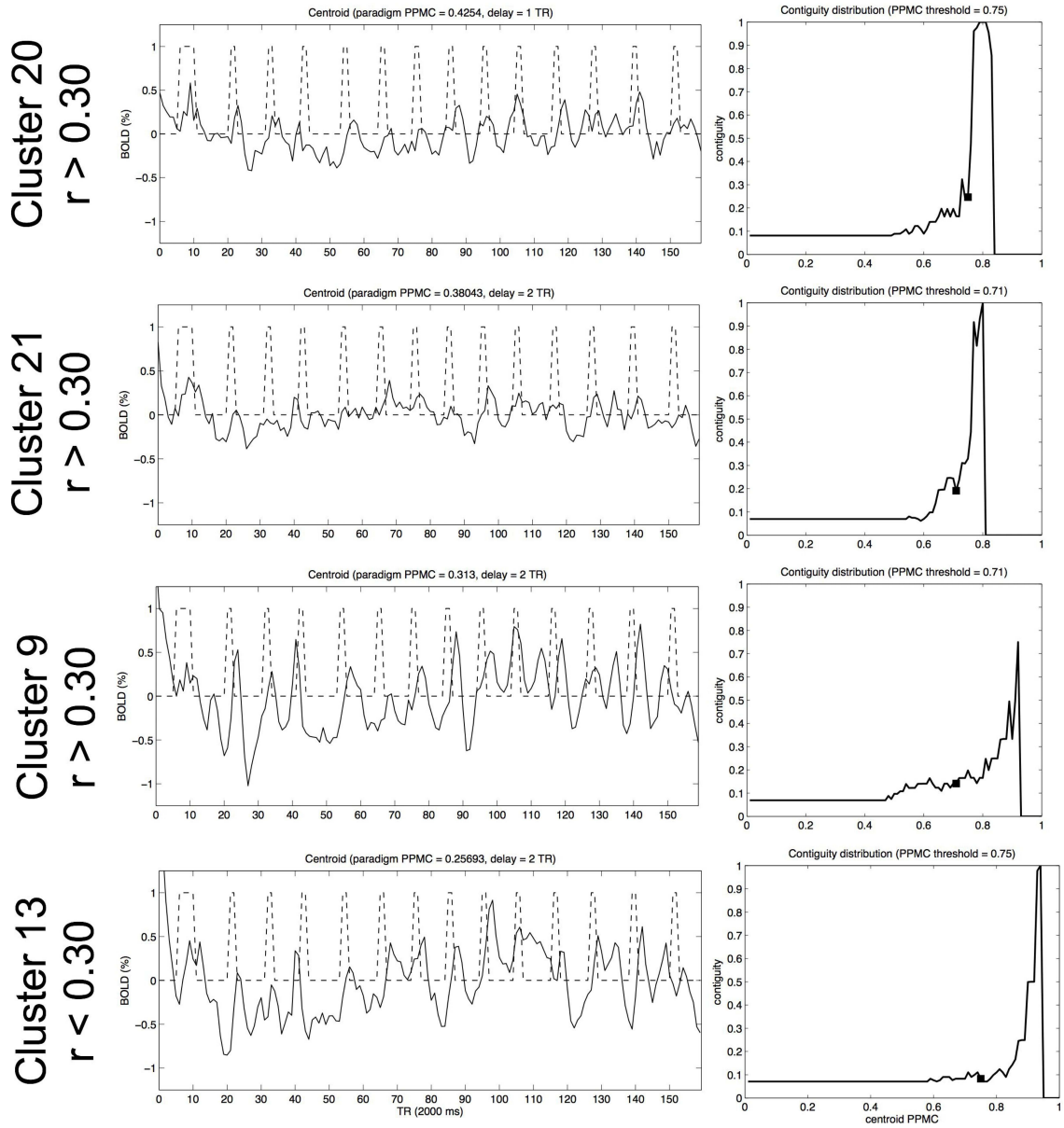

Figure 4: Corresponding cluster–paradigm correlation (*left*) and contiguity (*right*) plots for cluster maps in figure 3 selected from session 9 data. The paradigm (dashed) and centroid (solid) time-sequences are plotted *vs.* time in increments of 10 T_R (20 s). The contiguity distribution $c(r)$ is plotted *vs.* the voxel–centroid correlation. The r_{th} threshold is marked by the symbol '■'.